Effects of Alloying Elements on the Mechanical Properties and Corrosion Behaviors of 2205 Duplex Stainless Steels

Horng-Yih Liou, Yeong-Tsuen Pan, Rong-Iuan Hsieh, and Wen-Ta Tsai

(Submitted 29 October 1999)

The effects of alloying elements on the microstructure, mechanical properties, and corrosion behaviors of duplex stainless steels (DSSs) have been investigated in this study. Experimental alloys were prepared by varying the concentrations of the constituent elements in DSSs. Hot ductility test, tensile test, charpy impact test, and corrosion test were performed to evaluate the properties of the experimental alloys. The results showed that the extent of edge cracking of DSSs increased with the increasing value of the crack sensitivity index (CSI). The higher the hot ductility index (HDI) was, the better the hot ductility of DSSs achieved. Austenite (γ) stabilizer generally caused a decrease in the strength and an increase in the charpy impact absorbed energy of the stainless steel. On the contrary, ferrite (α) former exerted its beneficial effect on the strength but became detrimental to the toughness of DSSs. The presences of sulfur and boron also caused a decrease in the impact energy, but nitrogen and carbon hardly affected the toughness within the concentration range tested in this study. The value of pitting nucleation potential (E_{np}) of different nitrogen contents in 3.5 wt.% NaCl solution at room temperature was almost the same, but the value of pitting protection potential (E_{pp}) among these alloys was increased with increasing the content of nitrogen. The susceptibility to stress corrosion cracking (SCC) of DSSs was high when tested in boiling 45 wt.% $MgCl_2$ solution. On the other hand, the time to failure of the experimental steels in 40 wt.% $CaCl_2$ solution at 100 °C was longer than that in $MgCl_2$ solution. Nitrogen could affect the SCC behavior of DSSs in $CaCl_2$ solution through the combinative effects by varying the pitting resistance and the slip step dissolution. An optimum nitrogen (N) content of 0.15 wt.% was found where the highest SCC resistance could be obtained. Although γ phase exhibited better resistance to SCC, cracks were found to penetrate through α and γ grains or to propagate along the α/γ interface. As a result, a mixed transgranular plus intergranular mode of fracture surface was observed.

Keywords alloying elements, corrosion behaviors, crack sensitivity index, duplex stainless steel, hot ductility index, mechanical properties.

1. Introduction

It is well known that the duplex stainless steels (DSSs) possess high strength and excellent corrosion resistance, with relatively low cost. So, they are increasingly used as structure materials in many applications, such as offshore platforms, oil and gas production, chemical plants, pulp and paper industries, nuclear reactors, and process systems, where both high mechanical strength and high corrosive resistance are required.[1–6] A DSS is defined as one that contains a two-phase structure and is an Fe-Cr-Ni alloy, where both phases are present more than 30%.[7] The first study on this steel appeared in 1927, when Bain and Griffith published data on ferritic-austenitic structure.[8] Until now, many commercial DSSs, such as 2205, SAF2304, SAF2507, Ferralium 255, Zeron 100, DP3, *etc.*, have been developed.

Since the ferrite-austenite balance has a critical influence on the properties of DSS, determining a method to obtain an optimum combination of properties is very important and of great interest. It has been reported that strength, pitting corrosion resistance, intergranular corrosion resistance, and stress corrosion cracking (SCC) resistance decrease with increasing austenite content.[1,3,4] However, with increasing ferrite content, fracture toughness decreases and the possibility of σ phase embrittlement increases. Unfortunately, neither the austenite nor the ferrite content can be kept unchanged. Rather, they are affected by the alloying elements and the thermal history. The influence of alloying elements on the microstructurale changes, mechanical properties, and corrosion behaviors of DSSs has been an interesting subject for many researchers.[9–14] It is known that Cr and Mo are ferrite formers and Ni and N are austenite stabilizers. It has long been recognized that Cr is the major element used to form the passive film, which improves the localized corrosion resistance and oxidation resistance.[9,12] On the other hand, Ni has the function not only to control phase balance and element partitioning but also to improve mechanical property and anticorrosion in reducing acid.[9] The role of Mo is found to cause increases in the stability of the passive film and the pitting and crevice corrosion resistances. However, it also enhances the risk of intermetallic precipitation.[10,14] Nitro-

Horng-Yih Liou, and **Wen-Ta Tsai,** Department of Materials Science and Engineering, National Cheng Kung University, Tainan, 70101, Taiwan, Republic of China; and **Yeong-Tsuen Pan,** and **Rong-Iuan Hsieh,** Steel and Aluminum Research and Development Department, China Steel Corporation, Hsiao-Kang, Kaohsiung 81233, Taiwan, Republic of China. Contact e-mail: t113@mail.csc.com.tw.

Table 1 Chemical compositions of experimental stainless steels used in this study (wt.%)

Specimen	ID	C	Si	Mn	P	S*	Ni	Cr	Mo	N	Cu	B*
A	LMo	0.024	0.49	1.5	0.028	46	5.54	22	2.7	0.147	0.24	…
B	HMo	0.024	0.49	1.5	0.028	46	5.54	22	3.3	0.147	0.24	…
C	LCr	0.026	0.5	1.53	0.029	54	5.57	21.1	3.08	0.148	0.24	…
D	HCr	0.026	0.5	1.53	0.029	54	5.48	22.1	3.03	0.148	0.24	…
E	LNi	0.028	0.49	1.5	0.029	54	4.88	21.9	3.1	0.157	0.24	…
F	HNi	0.028	0.48	1.47	0.029	54	6.24	21.5	3.06	0.157	0.24	…
G	LCu	0.025	0.55	1.53	0.033	65	5.58	21.7	3.08	0.157	0.05	…
H	HCu	0.025	0.55	1.53	0.033	65	5.5	21.5	3.04	0.153	0.52	…
I	LN	0.023	0.54	1.45	0.032	52	5.8	22	3.06	0.103	0.24	…
J	HN	0.023	0.54	1.38	0.032	52	5.9	22.1	3.08	0.195	0.24	…
K	B1	0.025	0.5	1.53	0.03	52	5.64	21.8	3.01	0.158	0.24	22
L	B2	0.025	0.51	1.53	0.03	52	5.65	21.9	3.08	0.158	0.24	32
M	LC	0.013	0.53	1.45	0.032	52	5.78	21.9	3.1	0.154	0.24	…
N	Base 1	0.023	0.53	1.45	0.032	52	5.82	21.9	3.1	0.153	0.24	…
O	S1	0.025	0.57	1.47	0.029	80	5.69	21.7	2.99	0.15	0.24	…
P	S2	0.025	0.57	1.48	0.029	120	5.69	21.7	2.99	0.15	0.24	…

* S, B in ppm

gen has a multiple effect on DSSs by increasing pitting, crevice corrosion resistance, austenite content, and strength. It also retards the formation of intermetallic compound during phase transformation and in the heat-affected zone.[11,14]

Although the major effects of individual alloying elements on the mechanical properties and corrosion behaviors in DSS are recognized, the influence of the variation of alloy contents on these characteristics is not yet clear. Furthermore, the complex synergistic effects among alloy elements may exist but are seldom explored. Hence, in this study, the effects of different alloy elements and their concentration changes on the mechanical properties and corrosion behaviors of 2205 DSSs are systematically investigated.

2. Experimental Procedures

2.1 Materials

The experimental alloys with compositions close to that of 2205 duplex steels were prepared from 250 kg vacuum melt heats and cast as 160 × 160 mm square ingots. The chemical compositions of all experimental alloys are listed in Table 1 with 22Cr-5.8Ni-3.1Mo-1.54Mn-0.53Si-0.24Cu-0.15N-0.023C DSS as a reference. For steels A to J, Mo, Cr, Ni, Cu, and N contents were varied for mechanical properties and corrosion behaviors evaluations. For steels K to P, B, C, and S contents were varied for the investigations of mechanical properties and hot workability.

The ingots were reheated at 1250 °C for 1.5 h and hot rolled into plates with two different thickness, 13 and 5 mm, respectively. The as-rolled 13 mm thick plates were directly used for hot ductility testing. The 5 mm thick plates were subjected to a solution treatment at 1100 °C for 10 min followed by water quenching before specimen machining for tensile, charpy impact, and corrosion tests.

2.2 Hot Ductility Test

The specimens used for hot ductility testing were cut from 13 mm thick plates with their longitudinal direction parallel to the rolling direction. The gauge length is 20 mm. A Gleeble (New York, USA) 1500 thermomechanical simulator was used to evaluate the hot ductility of DSSs by on-cooling type high-temperature tensile testing.[15] Before being pulled to rupture at a stroke rate of 20 mm/sec, the specimens were first heated to 1250 °C at a rate of 20 °C/s and held for 10 min for solution treatment, then cooled at a rate of 10 °C/s to 1100 °C and 950 °C for 30 s. The hot ductility was determined in terms of reduction of area (RA) of broken specimens using the following equation:

$$RA\ (\%) = \frac{(d_0^2 - d^2)}{d_0^2} \times 100\%$$

where d_0 and d are the initial and final specimen diameters, respectively.

2.3 Pitting Corrosion Test

An EG&G (Princeton, NJ) PAR 273 potentiostat was employed to obtain the cyclic potentiodynamic polarization curves in 3.5 wt.% sodium chloride (NaCl) at room temperature. The potential scan rate was 1.67 mV/s. The reference electrode was a saturated calomel electrode. Carbon rods were used as the counter electrodes. For determining the pitting resistance of DSSs, the critical potentials for pit nucleation (E_{np}) and pitting protection potential (E_{pp}) were measured.

2.4 SCC Test

The U-bend specimen was used to evaluate the sensitivity of SCC of DSSs. The test solutions were boiling 45 wt.% magnesium chloride ($MgCl_2$) at 155 °C and 40 wt.% calcium chloride ($CaCl_2$) at 100 °C. The time to failure was recorded to represent the property of sample to SCC.

3. Results and Discussion

3.1 Hot Ductility

Figure 1 shows the appearance of the hot-rolled plates. The extent of edge cracking of DSS can be seen to increase with

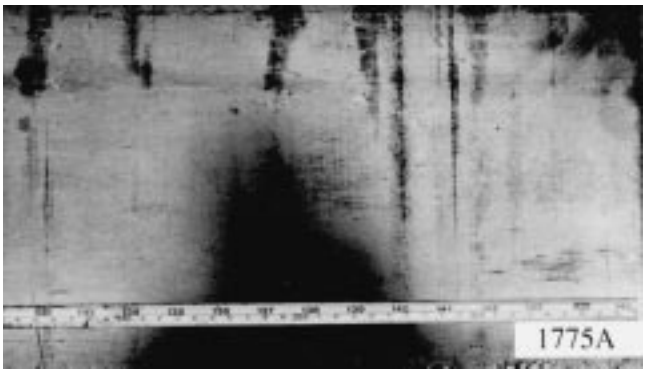

(**a**)

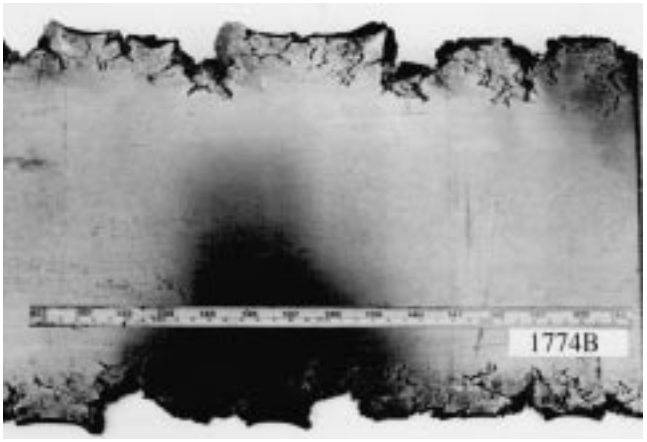

(**b**)

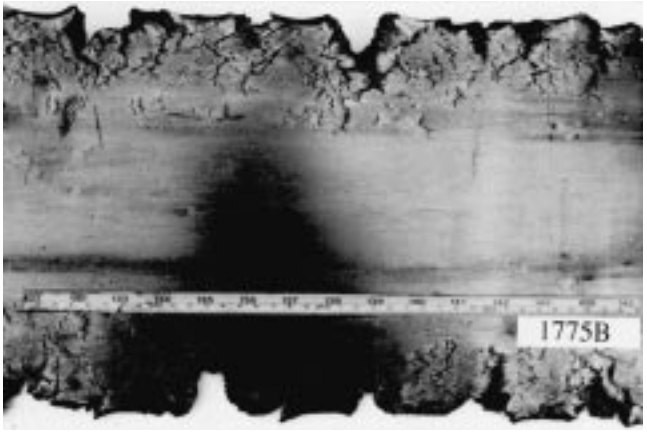

(**c**)

Fig. 1 The actual appearance of the hot-rolled plates of DSSs. (**a**) 0.1 wt.% N, (**b**) 0.153 wt.% N, and (**c**) 0.195 wt.% N

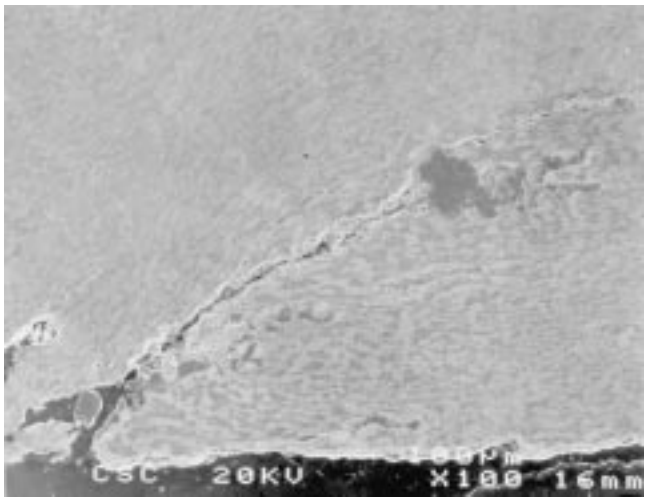

(**a**)

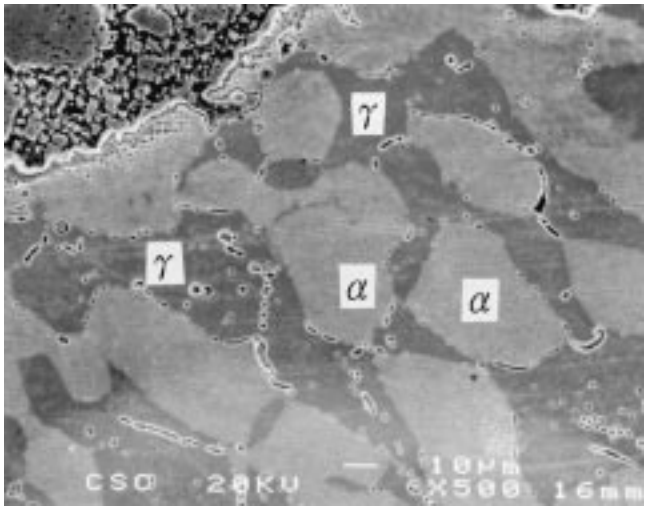

(**b**)

Fig. 2 (**a**) SEM micrographs of the edge cracking of stainless steel and (**b**) enlargement of Fig. (a)

increasing N content. The main reason is that the deformation resistances of α phase and γ phase are different at temperature range for hot rolling. The high-temperature strength of α phase is lower than that of γ phase, so the deformation of DSS is concentrated on α phase. Figure 2 shows the cross section of an edge crack. The crack initiated in the 45° shear direction of the plate and propagated either along α/γ interfaces or the intragranular of γ phase. This result demonstrates that γ phases are prone to cracking. Hence, the possibility of edge cracking increases with the increasing amount of γ phase resulting from high N content. A similar result was reported by Decroix *et al.*[16]

The occurrence of edge cracking would lead to a yield loss. Since a longer crack length would result in a greater yield loss, the extent of crack propagation is more important than the number of cracks initiated. The extent of edge cracking is strongly dependent upon the alloying elements and their concentrations. The dependence of edge crack length on the alloying elements may be expressed in terms of the crack sensitivity index (CSI), which is defined (using the multi-regression method) as follows:

$$\mathrm{CSI} = 45.2\mathrm{C} + 18.3\mathrm{N} + \mathrm{Mo} + \mathrm{Cu} + 0.65\mathrm{Ni}\text{-}297\mathrm{B}\text{-}0.14\mathrm{Cr}\text{-}0.7\mathrm{Mn}$$

where all the elements are in weight percent. The variation of

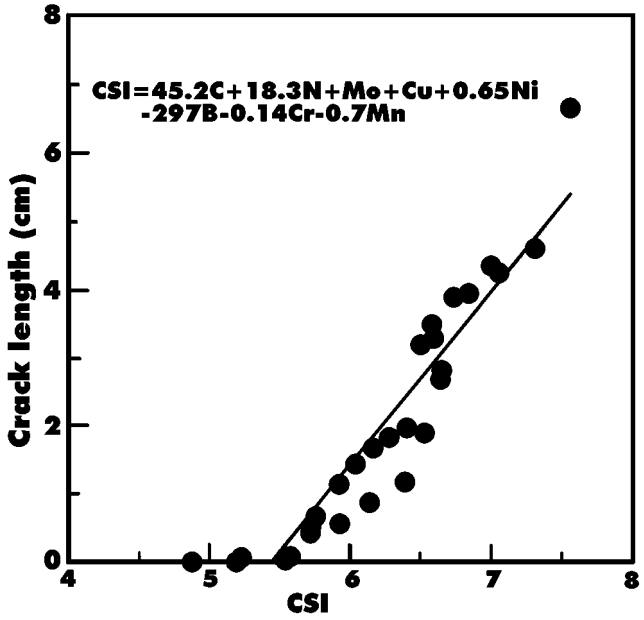

Fig. 3 Effect of CSI on the edge cracking of DSSs

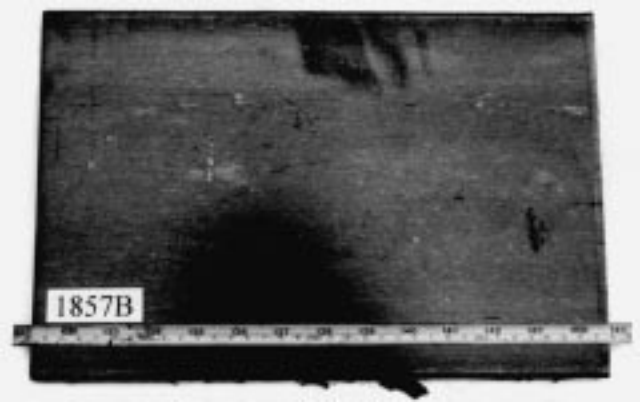

Fig. 4 The appearance of the hot- rolled plate of a DSS with less crack

edge crack length (estimated from the ten longest edge cracks) with CSI is shown in Fig. 3.

As can be seen in Fig. 3, the average crack length increases with increasing value of CSI. If the value of CSI was raised to more than 5.5, notable edge cracking of the DSSs would occur. From the above equation, it is clearly seen that Cr, Mn, and particularly B can reduce CSI, while C, N, Mo, Cu, and Ni are detrimental elements on the hot workability of DSSs. Based on the above observation, DSSs with proper alloy design to make CSI less than 5.5 are resistant to edge cracking, as can be seen from the example shown in Fig. 4. According to this alloy designed method, the DSS with less edge crack was obtained and is shown in Fig. 4.

Figure 5 demonstrates the effect of concentration change of the substitutional alloying element on the hot ductility of DSSs at 1100 °C. In Fig. 5, the concentration change of each alloying elements was determined with respect to the reference DSS, namely, Fe-22Cr-5.8Ni-3.1Mo-1.54Mn-0.53Si-0.24Cu-0.15N-0.023C. The negative sign of concentration change implies that

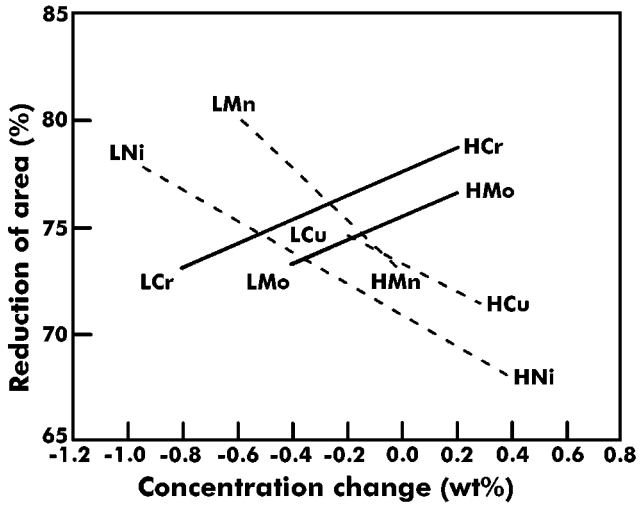

Fig. 5 Effect of concentration change of the substitutional alloying elements on the hot ductility of DSSs at 1100 °C

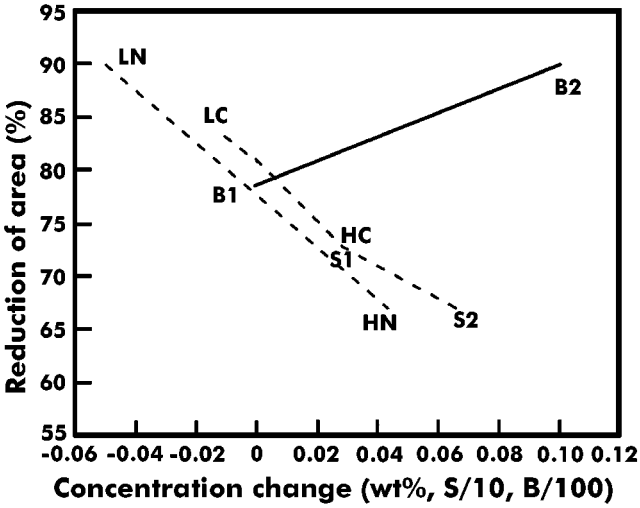

Fig. 6 Effect of minor alloying elements on the hot ductility of DSSs at 1100 °C

the content of a specific alloying element is lower than that of the reference alloy, and *vice versa*. It was found from this figure that the hot ductility increased as the contents of α formers, Cr and Mo, were increased. On the other hand, the hot ductility decreased with increasing the contents of γ stabilizers (Ni, Mn, and Cu). The influences of minor elements on the hot ductility of DSSs at 1100 °C are shown in Fig. 6. It was found that the hot ductility was impaired with increasing amounts of C, N, and S, but was enhanced as the B content was increased. Kobayashi *et al.*[17] have already pointed out that, with α phase greater than 20%, the hot ductility of DSS increased with increasing α phase content. In this study, the ferrite contents of DSSs were measured between 50 and 65%. The volume fraction of α would increase as the contents of α stabilizing elements (such as Cr and Mo) were increased, while it would decrease with increasing γ forming elements (such as Ni, Mn, and Cu). The experimental

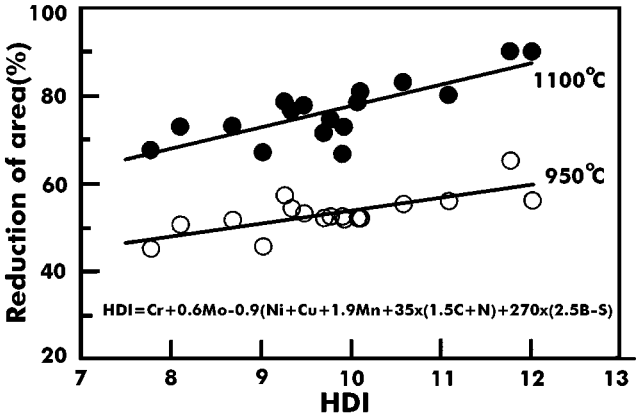

Fig. 7 Effect of HDI on the hot ductility of DSSs

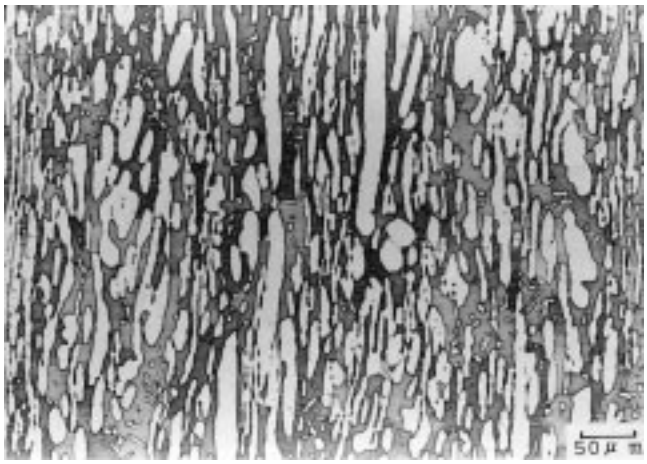

Fig. 8 Typical OM micrograph of a solution-treated DSS (0.153 wt.%)

results shown in Fig. 5 were consistent with that reported by Kobayashi *et al.*[17]

Fractographical examination after hot tension testing was performed. The results showed that the major crack path was along the α/γ interface. It is known that the impurities such as S, C, P, N, and O can easily segregate at the α/γ interfaces and weaken the interfacial strength and hot ductility.[16–18] The loss of hot ductility with increasing amounts of C, N, and S shown in Fig. 6 was not surprising. On the contrary, the segregation of B at the α/γ grain boundary can lead to the strengthening of the interfaces between α and γ phases.[19–21] The beneficial effect of B on hot ductility is also revealed in Fig. 6.

Based on the results of Fig. 5 and 6 and the above considerations, the amount of α phase and the grain boundary strength (σ_{GB}) are the most important factors determining the hot ductility of DSSs. Since both factors are dependent on the alloying elements and their concentrations, a new index (HDI = hot ductility index) is thus proposed and established to characterize the extent of hot ductility. Using the multi-regression technique, the relationship between RA and HDI is shown in Fig. 7. The definition of HDI is given below:

$$\begin{aligned}\text{HDI} &= \alpha \text{ content term} + \text{interfacial strength term}\\ &= \text{Cr} + 0.6\text{Mo} - 0.9\\ &\times (\text{Ni} + \text{Cu} + 1.9\text{Mn} + 35 \times (1.5\text{C} + \text{N}))\\ &+ 270 \times (2.5\text{B-S})\\ &= \text{Cr}_{eq} - 0.9\text{Ni}_{eq} + 270\sigma_{GB}\end{aligned}$$

Cr_{eq} is Cr + 0.6Mo, Ni_{eq} is Ni + Cu + 1.9Mn 35 × (1.5C + N), and σ_{GB} is 2.5B-S. All the elements in the above equation are in weight percent. The higher the HDI is, the better the hot ductility of DSS.

3.2 Mechanical Property

The typical microstructure of a solution-treated DSS is shown in Fig. 8. The etching solution is boiling Murukami reagent (10 g $K_3Fe(CN)_6$ + 10 g KOH + 100 mL H_2O), which makes the austenite appear white and the ferrite appear tanned. Figure 8 reveals that γ phase was embedded in the continuous α matrix. The entire matrix presents an elongated structure and has a strong texture in the rolling direction. Both α and γ grains were very fine. Because fine α and γ grains can enhance the strength and toughness of the steel,[1] the DSSs prepared in this study all possess very high strength and toughness.

Figures 9 and 10 show the effect of Cr_{eq} and Ni_{eq} on the mechanical properties of DSSs. The yield strength (YS) of DSS has the tendency to increase and the elongation to decrease with the increase of Cr_{eq}. However, with the increase of Ni_{eq}, the YS slightly decreases and the tensile strength and elongation increase. The reason is that the alloying elements of Cr_{eq} are α stabilizer, which can raise α content and promote the strength of stainless steel. On the other hand, the alloying elements of Ni_{eq} are γ stabilizer, which can raise γ content and reduce the strength of stainless steel. Besides, the α formers also cause a decrease in the stacking fault energy (SFE) of stainless steels and make the dislocations become difficult to climb and cross-slip, which consequently results in an increase in the strength of the materials. On the other hand, the γ formers give rise to an increase in the SFE and make the dislocations become easy to climb and cross-slip. Hence, the strength of the materials decreases with increasing Ni_{eq}.[22]

Because of the presence of α phase, DSS exhibits a ductile-to-brittle transition behavior. However, the facts of the small grain size and the presence of γ phase lead to a very low transition temperature. Figures 11 and 12 show the effects of nickel and molybdenum content of DSSs, respectively, on the impact absorbed energy. The absorbed energy increases with the increase of nickel content from 4.88 to 6.24% and decreases as the molybdenum content increases from 2.7 to 3.3%. All the transition temperatures are about −20 to −40 °C. Figures 13 and 14 demonstrate the effects of α and γ contents of DSSs on the absorbed energy. The average absorbed energy in room temperature is 200 joules. When the test temperature was decreased, the impact energy was also decreased. However, the absorbed energy was higher than 80 joules even if the testing temperature was below −100 °C. From these figures, it can also be found that the absorbed energy decreased slightly with increasing content of α phase.

In the experimental composition ranges, the influence of

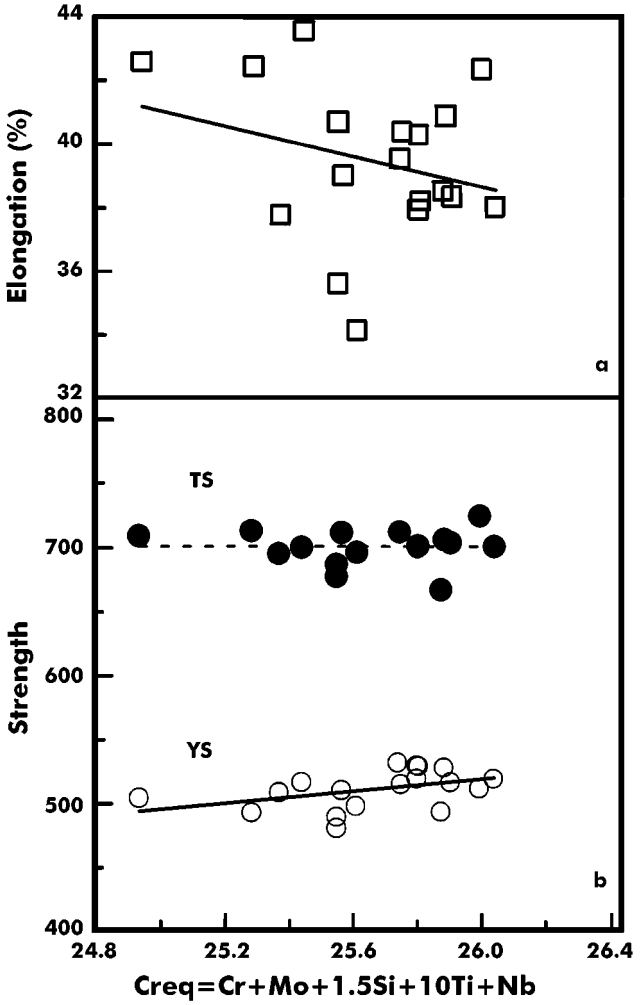

Fig. 9 Effect of Cr_{eq} of DSSs on the mechanical property: (**a**) elongation and, (**b**) strength

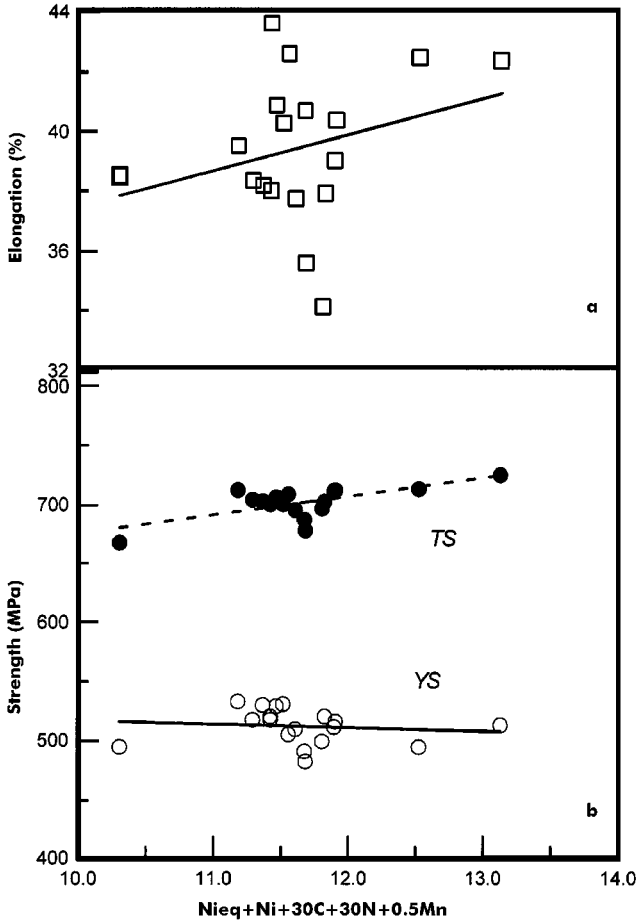

Fig. 10 Effect of Ni_{eq} of DSSs on the mechanical property: (**a**) elongation and, (**b**) strength

nitrogen content on impact energy is shown in Fig. 15. The ductile-to-brittle transition curves hardly change. All ductile-to-brittle transition temperatures are −20 °C. That means that the increase of N content (0.1 to 0.2%) does not cause an obvious decrease in the toughness of DSS until −100 °C. A similar result was found for the effect of carbon content (0.013 to 0.028%) on toughness. However, both sulfur (Fig. 16) and boron led to a decrease in the absorbed energy, especially at higher testing temperature.

3.3 Corrosion Behaviors

Pitting Corrosion. The cyclic potentiodynamic polarization curves of DSSs with three different nitrogen contents in 3.5 wt.% NaCl solution at room temperature are shown in Fig. 17. Wide passive ranges, from −500 to 1100 mV, were seen for these three experimental steels. The value of E_{np} was higher than 1100 mV for each alloy, indicating excellent resistance to pitting corrosion. Although pits were seldom seen after electrochemical polarization tests, they could be found by controlling potential at 1250 mV for 30 min. This result indicated that the

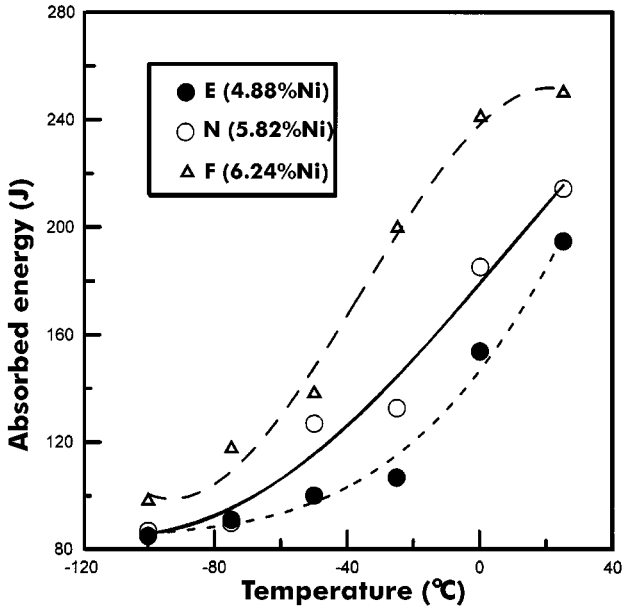

Fig. 11 Effect of nickel content of DSSs on impact absorbed energy

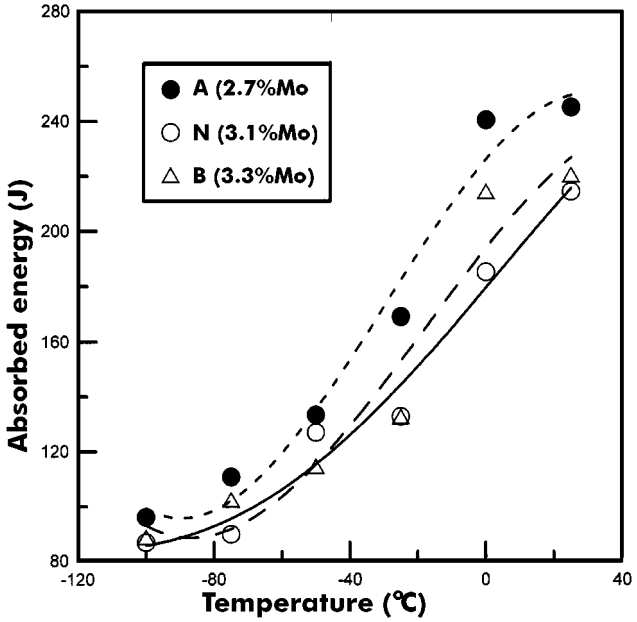

Fig. 12 Effect of molybdenum content of DSSs on impact absorbed energy

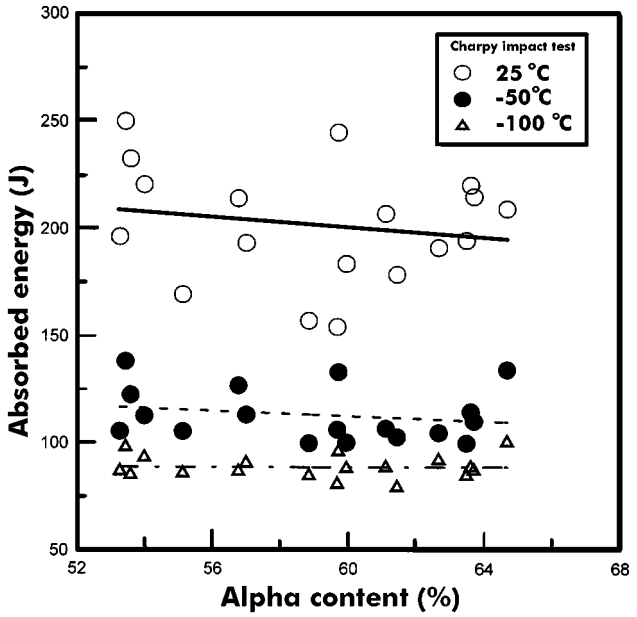

Fig. 13 Effect of alpha content of DSSs on the charpy impact energy

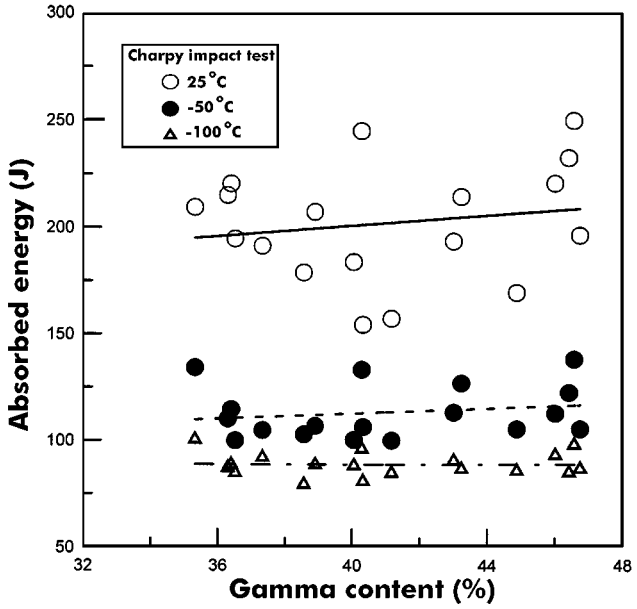

Fig. 14 Effect of gamma content of DSSs on the charpy impact energy

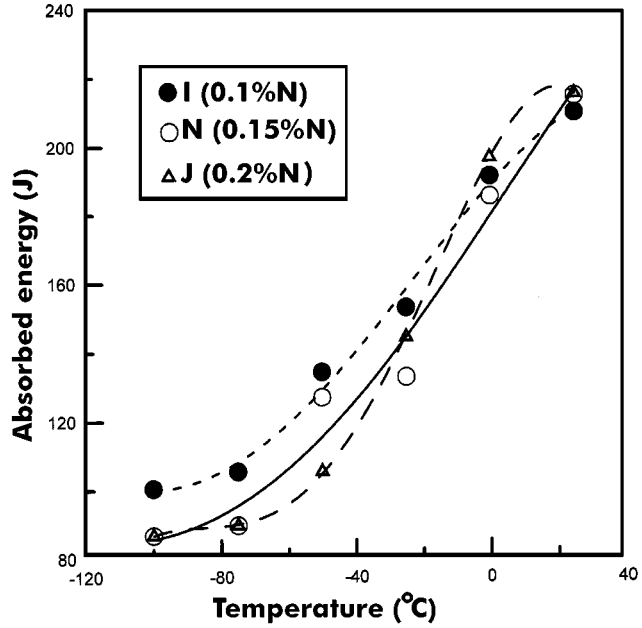

Fig. 15 Effect of nitrogen content of DSSs on impact absorbed energy

pitting potential is similar to the transpassive potential of DSSs. In Fig. 17, it could also be found that the value of E_{np} of each of the three experimental steels was almost the same. But, differences in the passive current density and E_{pp} among different alloys were observed. The greater the N content is, the higher the E_{pp}.

The E_{pp} of low N (0.1% N) stainless steel was about −200 mV; however, the E_{pp} of high N (0.2% N) DSSs was 1050 mV, which was close to E_{np}. The result indicated that the addition of N could raise pitting corrosion resistance of DSSs. It has been indicated that nitrogen can be enriched in the interface between the metal and the oxide, and form NH_4^+ or Ni_2Mo_3N on the specimen surface to generate high passive film.[14] The beneficial effect of N on improving the pitting resistance of stainless steels is well recognized.

Stress Corrosion Cracking. The effects of nitrogen contents on SCC behavior of DSSs in 45% $MgCl_2$ and 40% $CaCl_2$ solutions, respectively, are shown in Fig. 18. It can be seen that the time to failure of experimental steels in boiling 45%

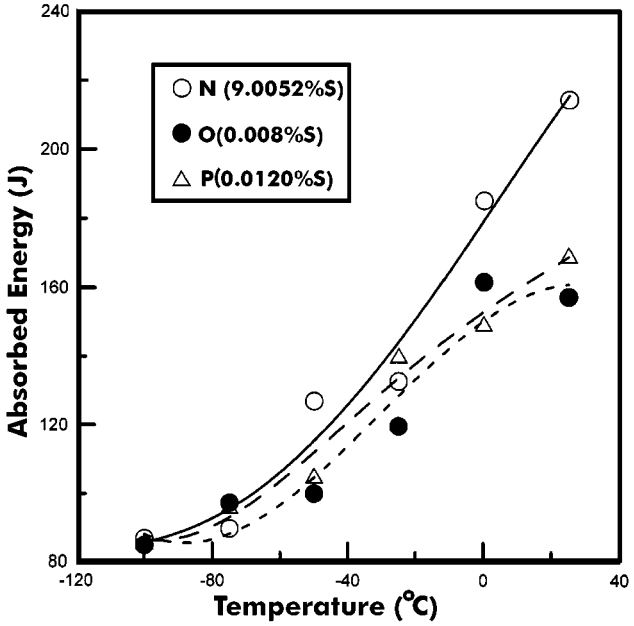

Fig. 16 Effect of sulfur content of DSSs on impact absorbed energy

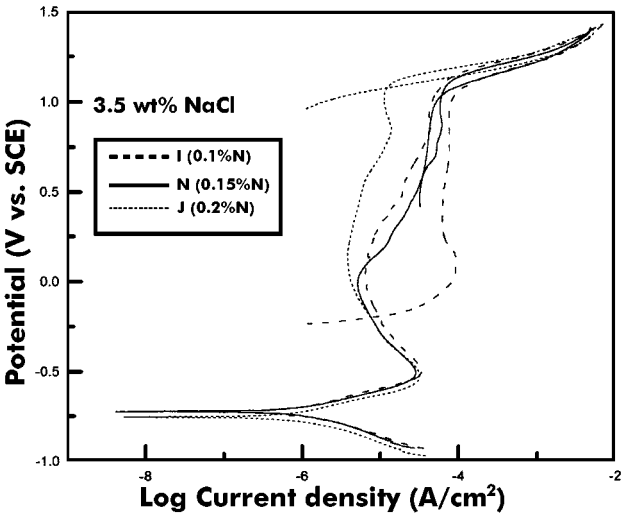

Fig. 17 Cyclic potentiodynamic polarization curves of three nitrogen contents of DSSs in 3.5 wt.% NaCl solution

$MgCl_2$ solution was short (less than 3 hr), no matter what the N content was. This result indicated that the susceptibility of DSSs to SCC is high in boiling $MgCl_2$ solution. On the other hand, the time to failure of each experimental steel in 40% $CaCl_2$ (100 °C) solution was longer than that in $MgCl_2$ solution. The maximum value of failure time was found for the steel with a N content of 0.15%.

It is well known that the chloride ion is aggressive for the occurrence of SCC for many alloys in aqueous environments. In addition to chloride content and pH value, cations also play important roles in SCC. Cations can affect both the activity of the chloride ion and the solubility of oxygen in solution. They also influence the hydrogen ion activity, the composition of the

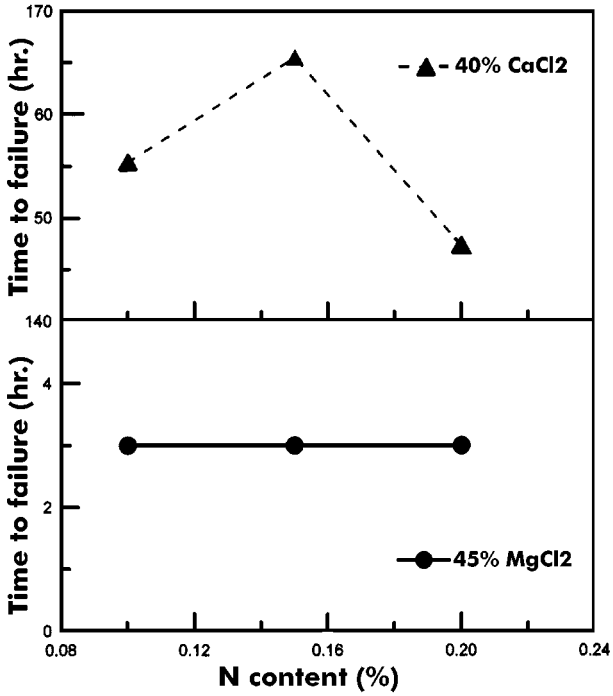

Fig. 18 Effects of nitrogen contents of DSSs on SCC behavior in 45% $MgCl_2$ and 40% $CaCl_2$ solutions

passive film, and the surface mobility.[23] Generally, the ability of cation to initiate SCC in chloride solution varies in the following order: $Mg^{2+} > Fe^{3+} > Ca^{2+} > Na^{+} > Li^{+}$. In other words, $MgCl_2$ solution is the most aggressive solution among the chloride solutions considered. The rather short time to failure of DSS in boiling $MgCl_2$ solution is thus not unexpected.

According to Berhardsson,[24] the 40% $CaCl_2$ solution has been suggested to be the optimum SCC test solution for molybdenum bearing stainless steels in comparison with the practical application. The use of $CaCl_2$ solution has some advantages over $MgCl_2$ solution. More specifically, $CaCl_2$ solution is not too severe in comparison with the environments usually encountered in the industries. Furthermore, the solution pH can be easily adjusted so that the distinction between hydrogen-assisted cracking and pitting-induced cracking can be made.[25]

After SCC test (U-bend test), each specimen surface was examined under scanning electron microscopy (SEM). Figure 19 gives the surface appearances of two experimental steels with different N content. The SEM micrographs reveal that extensive pits were formed on the specimen surface. The pit depth on the surface of the low nitrogen content (0.1 wt.%) DSS is higher than that with high nitrogen content (0.15 wt.%). The formation of corrosion pits on the surface might thus assist the initiation of crack. It is known that pitting resistance increases with N content in DSS. The steel with 0.1 wt.% N would be more susceptible to pitting corrosion, as compared with the steel containing 0.15 wt.% N, and subsequently, it more easily enhanced the crack initiation in 40 wt.% $CaCl_2$ solution at 100 °C. The difference in time-to-failure for SCC test for the above two steels with different N content is revealed in Fig. 18. The time to failure for the steel containing 0.20 wt.% N, however, was short than that containing 0.15 wt.% N

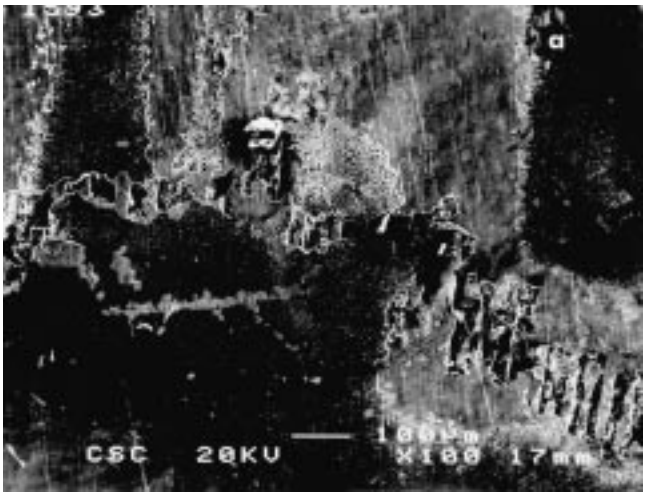

(**a**)

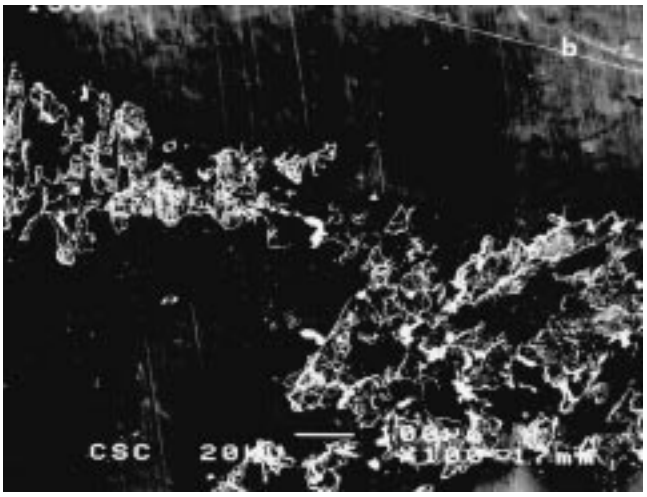

(**b**)

Fig. 19 Surface SCC crack induced by pitting corrosion in 40 wt.% $CaCl_2$ solution: (**a**) 0.1 wt.% N and, (**b**) 0.153 wt.% N

(also revealed in Fig. 18). The possible explanation is given below.

The slip dissolution mechanism is generally applied to explain the SCC behavior of the passivated alloys such as stainless steels.[26] If the process of slip step, a result of dislocation movement, in an alloy can take place easily, according to the slip dislocation model, this material may be more susceptible to SCC. For an alloy with low (SFE), the separation between two partial dislocations will be relatively broad, which means that the steps on the surface will be sufficiently large to be able to rupture the passive layer.[23] As a consequence, an alloy will be more susceptible to SCC if its SFE decreases. According to Pickering,[27] the SFE of a stainless steel varies with its composition by the following equation:

$$\text{SFE (mJ/m}^2\text{)} = 25.7 + 2\text{Ni} + 410\text{C-0.9Cr-77N-13Si-1.2Mn}$$

As shown in the above equation, SFE can be substantially

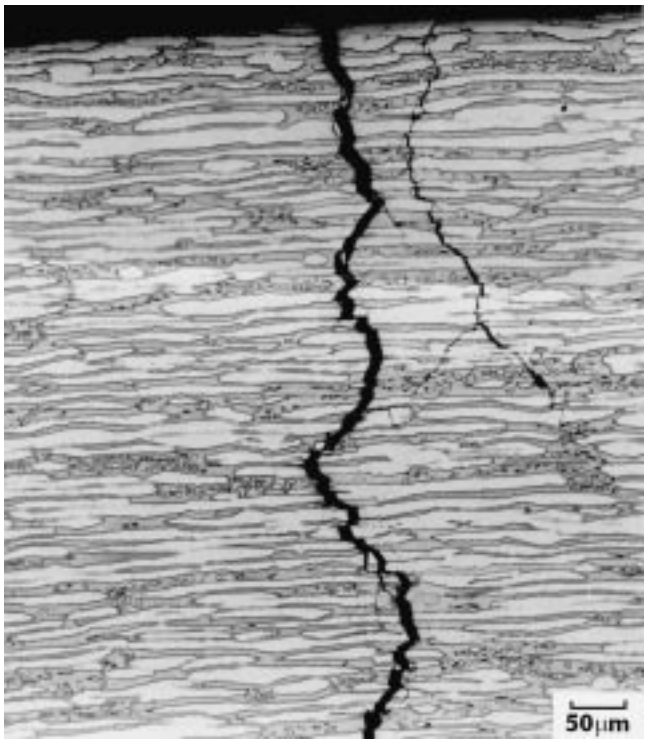

Fig. 20 The SCC propagation path of a DSS in boiling 45 wt.% $MgCl_2$ solution

reduced with the alloying of N. If the nitrogen content is raised, the SFE of the steel is decreased. Accordingly, the DSS with 0.15 wt.% N has a higher SFE than that of 0.20 wt.% N steels. Hence, the SCC resistance of the former was higher than that of the latter, provided that pitting assisted crack initiation was not dominant in the SCC process.

Figure 20 shows the SCC propagation path in an experimental steel in boiling 45% $MgCl_2$ solution. No pitting corrosion was observed for the specimen tested in boiling $MgCl_2$ solution. Crack could penetrate through the ferrite and the austenite grains or propagate along the interfaces between them. The mixed transgranular and intergranular fracture morphology was also revealed in the SEM fractograph, as shown in Fig. 21(a). Similar observations were found for the experimental steels tested in $CaCl_2$ solution, while pits acted as the crack initiation sites (Fig. 21b).

The roles of ferrite and austenite on the crack blocking effect in DSSs have long been of interest because of the controversial observations reported. In earlier times, Edeleanu.[28] Flowers *et al.*,[29] and Hochmann *et al.*[30] all reported that ferrite was anodic to austenite in DSSs. Thus, the increase of ferrite content could raise the SCC resistance of the steels.[31] However, it was found in recent studies[32,33] that crack occurred preferentially in the ferrite matrix and the austenite acted as a crack barrier. According to Kangas and Nicholls[23] and Bemhardsson *et al.*,[31] ferrite could block cracking in DSS at low stress. They also found that cracks propagated intergranularly at intermediate stress, while they propagated transgranularly through both ferrite and austenite grains at high stress. The roles of ferrite and austenite in the crack propagation processes are complicated and probably attribute to the difference in test conditions, including

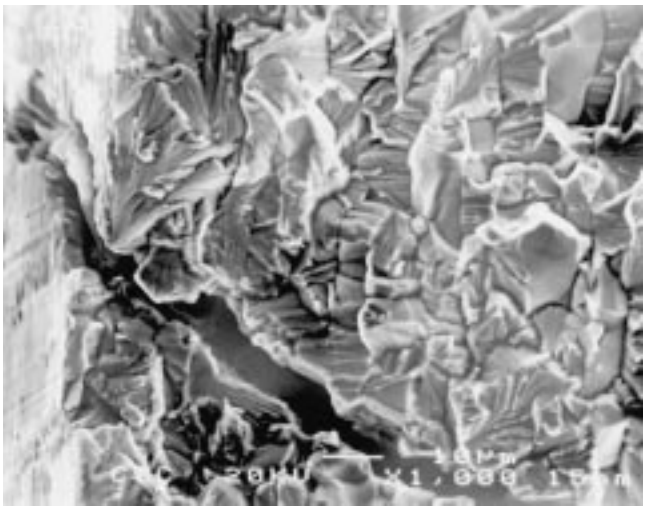

(**a**)

(**b**)

Fig. 21 SEM micrographs of SCC fracture surface of DSS in (**a**) boiling 45 wt.% $MgCl_2$ and (**b**) 100 °C 40 wt.% $CaCl_2$ solution

stress states, test environments, alloying elements, *etc.* Most observations, however, lead to the same conclusion that the DSSs have better resistance to chloride-induced SCC than the corresponding ferrite and austenite stainless steels.

4. Conclusions

The conclusions of this investigation may be summarized as follows.

- The edge cracking of DSS increases with increasing value of CSI. When the value of CSI is higher than 5.5, the stainless steel is susceptible to edge crack.
- The α content and the bonding strength of the grain boundary are the most important factors affecting hot ductility. The higher the HDI is, the better the hot ductility of DSS.
- Austenite stabilizer decreases the strength and promotes the absorbed energy of stainless steel. On the contrary, α former exerts its beneficial effect on the strength and exhibits an inferior result on the absorbed energy as compared with γ stabilizer. The sulfur and boron also decrease the absorbed energy, but the nitrogen and carbon hardly affect the toughness within the concentration range tested in this study.
- The value of E_{np} is higher than 1100 mV for experimental steels in 3.5 wt.% NaCl solution at room temperature, indicating excellent pitting resistance. However, the value of E_{pp} among these alloys is increased with increasing nitrogen content.
- The susceptibility of DSS to SCC in boiling $MgCl_2$ solution is high. On the other hand, the time to failure of the experimental steels in 40 wt.% $CaCl_2$ solution at 100 °C is longer than that in $MgCl_2$ solution. The effects of nitrogen content of DSS on SCC behavior in $CaCl_2$ solution are the competitive results with pitting resistance and slip step dissolution. An optimum nitrogen content of 0.15 wt.% is found where the highest SCC resistance can be obtained. Cracks can penetrate through α and γ grains or propagate along the α/γ interface. Therefore, a transgranular plus local intergranular fracture mode of SCC morphology is observed.

References

1. J.O. Nilsson: *Mater. Sci. Technol.,* 1992, vol. 8, pp. 685-700.
2. J.P. Hoffman: *J. S. Afr. Inst. Mining Metall.,* 1986, vol. 86 (11), pp. 433-42.
3. K. Ravindranath and S.N. Mailhotra: *Corr. Sci.,* 1995, vol. 37 (1), pp. 121-32.
4. H.D. Solomon and T.M. Devine: in *Duplex Stainless Steels,* R.A. Lula, ed., ASM, Metals Park, OH, 1982, pp. 693-756.
5. R.D. Kane: *Adv. Mater. Processes,* 1993, vol. 144 (1), pp. 16-20.
6. J. Oredsson and S. Bernhardsson: *Mater. Performance,* 1983, vol. 22, pp. 35-42.
7. M. Barteri and F. Mancia: *Corrosion,* 1987, vol. 43, pp. 518-25.
8. E.C. Bain and W.E. Griffiths: *Trans. AIME,* 1927, vol. 75, pp. 166-213.
9. R.N. Gunn: *Duplex Stainless Steels-Microstructure, Properties and Applications,* Abington Publishing, 1997, pp. 14-19.
10. B. Walden and J.M. Nicholls: Sandvik Steel Technical Report No. S-51-53-ENG, Sandvik Steel, Köping, Sweden, 1994, pp. 1-12.
11. K. Ogawa, M. Miura, and Y. Komizo: *Q. J. Jpn. Welding Soc,* 1991, vol. 9 (2), pp. 269-75.
12. L.F. Garfias-Mesias, J.M. Sykes, and C.D.S. Tuck: *Corr. Sci.,* 1996, vol. 38, pp. 1319-30.
13. K.Y. Kim, P.O. Zhang, T.H. Ha, and Y.H. Lee: *Corrosion,* 1998, vol. 54 (11), pp. 910-21.
14. C.A. Olsson: *Corr. Sci.,* 1995, vol. 37 (3), pp. 467-79.
15. B. Ahblom and R. Sandstrom: *Int. Met. Rev.,* 1982, No. 1, pp. 1-27.
16. J.H. Decroix, A.M. Neven, and R.J. Castio: in *Deformation under Hot Working Condition,* ISI Publication, London, UK, 1968 p. 108.
17. H. Kobayashi, S. Yamaguchi, and M. Endo: in *Hot Working and Forming Process,* C.M. Sellars and G.J. Davies, eds., TMS, Warrendale, PA, 1979, pp. 133-39.
18. R. Nemoto, K. Osozawa, K. Osada, and M. Tsuda: in *Stainless Steels '84,* The Institute of Metals, London, UK, 1984, pp. 149-57.
19. B.J. Thomas and G. Henry: in *Boron in Steels,* S.K. Banerji and J.E. Morral, eds., AIME, Warrendale, PA, 1979, pp. 80-105.

20. S.R. Keown: in Ref. 17, pp. 140-47.
21. R. Otterberg and W. Roberts: in *Stainless Steels '84*, The Institute of Metals, London, UK, 1984, pp. 229-39.
22. N. Ohkubo, K. Miyakusu, Y. Uematsu, and H. Kimura: *Iron Steel Inst. Jpn. Int.*, 1994, vol. 34 (9), pp. 764-72.
23. P. Kangas and J.M. Nicholls: *Mater. Corr.*, 1995, vol. 46, pp. 354-65.
24. S. Bernhardsson: Sandvik Steel Report No. S-51-32-ENG, Sandvik Steel, Köping, Sweden, 1984, pp. 1-8.
25. T. Shibata, T. Harana, and T. Taniguchi: *10th APCCC, Proc. Books*, Indonesia, 1997, B. Widyanto, I. Nurdin, S. Wiryolukito, H. Ardy, R. Nasoetion, M. Sahari Besari, R. Suratman, A. Sulaeman, S. Purwadaria, S. Suprianto, S. Rachmat, and D.R. Munaf, eds., no. E2, INDOCOR, Bali, Indonesia, 1997.
26. R.W. Staehle: *The Theory of Stress Corrosion Cracking in Alloys*, J.C. Scully, ed., NATO, Brussels, Belgium, 1971, pp. 221-88.
27. F.B. Pickering: *Stainless Steels '84*, The Institute of Metals, London, UK, 1984, pp. 2-28.
28. C. Edeleanu: *J. Iron and Steel Inst.*, 1953, vol. 173, pp. 140-146.
29. J.W. Flowers, F.H. Beck, and M.G. Fontana: *Corrosion*, 1963, vol. 19, pp. 186t-198t.
30. J. Hochmann, A. Desestret, P. Jolly, and R. Mayoud: *Stress Corrosion Cracking and Hydrogen Embrittlement of Iron Base Alloys*, J. Hochmann and R.W. Staehle, eds., NACE, Houston, TX, 1977, pp. 956-1002.
31. S. Bernhardsson, J. Oredsson, and C. Martenson: in *Duplex Stainless Steels*, R.A. Lula, ed., ASM, Metals Park, OH, 1982, pp. 267-76.
32. W.J.R. Nisbet, R.C. Newman, and G.W. Lorimer: in *Duplex Stainless Steels*, Scotland, 1994, paper no. 126.
33. K. Takizawa, Y. Shimizu, E. Yoneda, and I. Tamura: *Trans. Iron Steel Inst. Jpn.*, 1982, vol. 22 (5), pp. 325-32.